

## Manipulating the steady-state entanglement via three-level atoms in a hybrid levitated optomechanical system


Guoyao Li,<sup>1</sup> Wenjie Nie ,<sup>1,\*</sup> Yu Wu,<sup>1</sup> Qinghong Liao,<sup>2</sup> Aixi Chen,<sup>3,†</sup> and Yueheng Lan<sup>4,‡</sup>

<sup>1</sup>*Department of Applied Physics, East China Jiaotong University, Nanchang 330013, China*

<sup>2</sup>*Department of Electronic Information Engineering, Nanchang University, Nanchang 330031, China*

<sup>3</sup>*Department of Physics, Zhejiang Sci-Tech University, Hangzhou 310018, China*

<sup>4</sup>*Department of Physics, Beijing University of Posts and Telecommunications, Beijing 100876, China*

 (Received 18 March 2020; revised 29 October 2020; accepted 9 November 2020; published 1 December 2020)

We theoretically investigate the generation of steady-state entanglement in a levitated optomechanical system with a cascade three-level atomic medium and a dielectric nanosphere. There are two cavity modes, driven by two external laser beams with different frequencies, which are responsible for trapping and cooling the nanosphere. Atoms prepared in coherent superposition are injected into the cavity to manipulate the optical fields and the effective optomechanical coupling. We show that the entanglement between the nanosphere and the cavity modes can be enhanced by selecting properly the initial population of the lower atomic level. In particular, when the atoms are prepared at that level, the corresponding optomechanical entanglement increases with the increase of the atom-field coupling strength. We also investigate in detail the influence of the effective cavity field detunings, the atomic detunings, the driving power, and the nanosphere's radius and found that there exist optimal values of the effective cavity field detuning and the driving power that maximize the optomechanical entanglement. By selecting the system's parameters properly, we further demonstrate the generation of genuine tripartite entanglement between three degrees of freedom in the system. The findings here may help flexible control of the steady-state entanglement in hybrid optomechanical systems.

DOI: [10.1103/PhysRevA.102.063501](https://doi.org/10.1103/PhysRevA.102.063501)

### I. INTRODUCTION

Cavity optomechanical system is usually designed to realize the coupling of macroscopic mechanical oscillator and cavity field [1–3]. In such optomechanical systems, the mechanical oscillators can take many forms, such as a movable mirror as the boundary of the cavity [4,5], an embedded dielectric membrane [6–8], a suspended nanosphere [9–13], or a microresonator in a microwave transmission line resonator [14]. Physically, these interactions between light and mechanical motion in cavity optomechanical systems are the result of the frequency of driven cavity mode changing with the position of mechanical oscillator, which serves as the basis for the high-accuracy measurement [15,16] and the sensing technology [17–19]. Further, based on the optomechanical coupling effect, the cavity optomechanical system can vividly display the quantum-mechanical effects in macroscopic systems, such as the photon blockade [20], optomechanically induced transparency (OMIT) [2], two-mode squeezing in the oscillation quadratures [21], ground-state cooling [22–27] and quantum coherence [28,29] of the mechanical mode, and so on. Moreover, the steady-state quantum entanglement between the mechanical and optical modes can be generated by the optomechanical coupling in various optomechanical setups [30–41], which has paved the way for quantum computation and quantum information processing [42–46].

In general, the optomechanical interaction between the light field and mechanical motion can be effectively enhanced by the external pump laser, which is helpful to embody the quantum effect of mechanical motion [1]. In addition to the enhancing effective optomechanical coupling by pumping light field, it can be also indirectly changed through the interaction between the internal state of atoms and the cavity field, so that the atomic ensemble placed in the cavity can be used to manipulate and enhance the quantum optomechanical entanglement [47–51]. Other optomechanical phenomena, such as OMIT [52–54] and high-order sideband generation [55–57], have been studied extensively based on atom-assisted hybrid optomechanical systems. In particular, the vacuum effect of the quantum emitter and its nearby mechanical oscillator can be used to mediate an effective optomechanical coupling between the mechanical oscillator and the cavity field [58] and manipulate the quantum optomechanical entanglement between a movable mirror and a light field [59]. Similarly, when a dielectric nanosphere is trapped near the cavity mirror, the vacuum interaction between them can enhance the quantum entanglement between the mechanical mode and optical fields [60,61]. Furthermore, the hybrid systems composed of a dielectric nanosphere and a two-level atomic ensemble have been established to study the macroscopic quantum mechanical motion, where the low-atomic excitation limit can be broken so that the steady-state optomechanical entanglement increases with increasing numbers of excited atoms [62].

In this work, a hybrid levitated optomechanical system composed of a cascade three-level atomic ensemble and a dielectric nanosphere is considered, which is driven by two

\*niewenjiezh@ sina.cn

†aixichen@zstu.edu.cn

‡lanyh@bupt.edu.cn

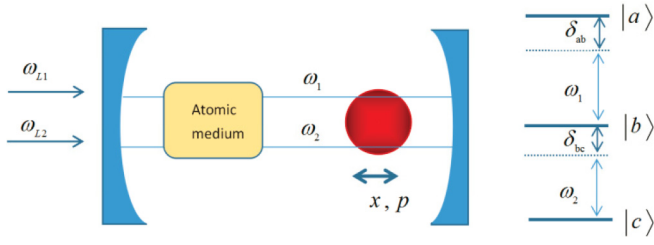


FIG. 1. Optomechanical system with a levitated dielectric nanosphere and a three-level cascade atomic medium with the levels of  $|a\rangle$ ,  $|b\rangle$ , and  $|c\rangle$ . The cavity field with frequency  $\omega_1$  ( $\omega_2$ ) is excited by the external driving laser with frequency  $\omega_{L1}$  ( $\omega_{L2}$ ). The nanosphere is trapped and levitated in the cavity by the optical potential of the driven cavity modes.  $x$  and  $p$  are the position and the momentum of the nanosphere, respectively. The atomic medium is coupled to the cavity fields with the detunings  $\delta_{ab}$  and  $\delta_{bc}$ .

external laser beams. Atoms prepared in a coherent superposition state are injected to the cavity and used to manipulate the optomechanical interaction between the levitated dielectric nanosphere and the two driven cavity fields. Then, based on the Heisenberg equations of motion and a linearization technology [30,63], the steady-state optomechanical entanglements between the dielectric nanosphere and the optical modes are analyzed in detail. We show that the optimal bipartite entanglement between the dielectric nanosphere and the optical mode 1 or 2 can be obtained under the appropriate effective cavity detuning and driving power. The influence of the initial population of the atomic states, the atomic detuning, the atom-field coupling strength, and the radius of the nanosphere on the steady-state optomechanical entanglement is also discussed in detail. In particular, we find that the levitated dielectric nanosphere and the two cavity modes can be entangled with each other with proper parameters of the system and therefore genuine tripartite entanglement between the levitated dielectric nanosphere and the cavity modes is realized.

The paper is organized as follows. In Sec. II, we present the model Hamiltonian, derive the Heisenberg-Langevin equation for the system, and study the quantum dynamics of the fluctuations around the steady-state value. In Sec. III, we evaluate the oscillation frequency of the levitated nanosphere and study the dependence on the system parameters of the optomechanical entanglement between the nanosphere and the cavity modes. Section IV presents a short summary of the paper.

## II. THE MODEL AND HAMILTONIAN

The hybrid optomechanical system studied here, which consists of a levitated nanosphere and an atomic medium with a cascade configuration injected into the cavity [49,64], is depicted in Fig. 1. Further, we consider that the Fabry-Pérot cavity is driven by two laser beams with frequencies  $\omega_{L1}$  and  $\omega_{L2}$  so that the trap and cooling of the nanosphere can be realized by the optomechanical interactions [64]. Correspondingly, the three-level atomic medium in the cavity interacts with the two-mode cavity fields with the detunings  $\delta_{ab}$  and  $\delta_{bc}$ , respectively, where  $|a\rangle$ ,  $|b\rangle$ , and  $|c\rangle$  denote the atomic states. We aim to investigate the entanglement between the levitated

nanosphere and the cavity modes for the continuous-variable optomechanical system, and study the influence of the three-level atomic medium on the entanglement with the help of the Heisenberg equation of motion of the system.

To this end, we first describe the Hamiltonian of the hybrid system, which can be written as [49,64]

$$\begin{aligned}
 H = & \sum_{j=1,2} \hbar \omega_j a_j^\dagger a_j + \frac{p^2}{2m} + \hbar \sum_{i=a,b,c} E_i \sigma_{ii} \\
 & + \hbar (G_1 \sigma_{ba} a_1^\dagger + G_2 \sigma_{cb} a_2^\dagger + \text{H.c.}) \\
 & - \hbar g_1 a_1^\dagger a_1 \cos^2(k_1 x) - \hbar g_2 a_2^\dagger a_2 \cos^2(k_2 x - \varphi) \\
 & + \sum_{j=1,2} i \hbar (\varepsilon_j a_j^\dagger e^{-i\omega_{Lj} t} - \varepsilon_j^* a_j e^{i\omega_{Lj} t}), \quad (1)
 \end{aligned}$$

where the first term in the first line describes the energy of the driven cavity modes and  $a_j$  ( $j = 1, 2$ ) is the photon annihilation operator for the  $j$ th cavity mode of frequency  $\omega_j = k_j c$ .  $k_j$  and  $c$  are the wave vector and the speed of light in vacuum, respectively. The second term in the first line is the kinetic energy of the levitated nanosphere at oscillation frequency  $\omega_m$ , which in general depends on the mass ( $m$ ) of the nanosphere and the steady-state values of the system [60,64]. The position  $x$  and momentum  $p$  for the center of mass (c.m.) of the nanosphere satisfy the commutation relations  $[x, p] = i\hbar$ . The third term in the first line is the free Hamiltonian of the atomic medium, where each atom is modeled by a three-level system with the excited states  $|a\rangle$  and  $|b\rangle$  and the ground state  $|c\rangle$ . Here we describe each atom in the medium by the spin operators  $\sigma_{i'i} = |i\rangle\langle i'|$  [ $i(i') = a, b, c$ ]. The terms in the second line describe the interactions of the atomic medium with the driven cavity fields, where  $G_j$  represents the averaged atom-field coupling strength [49]. The terms in the third line describe the interaction between the trapped nanosphere and the two cavity modes and  $g_j = \frac{3V}{4V_{c_j}} \frac{\epsilon-1}{\epsilon+2} \omega_j$  is the optomechanical coupling strength between the nanosphere and the cavity mode  $j$ , where  $V$  and  $V_{c_j}$  are the volumes of nanosphere and the optical mode  $j$ , respectively.  $\epsilon$  is the dielectric constant of the levitated nanosphere.  $\varphi$  is the phase between the two optical potentials. Finally, the term in the last line describes the interaction between the cavity modes and driving lasers with the amplitude  $|\varepsilon_j| = \sqrt{2P_j \kappa_j / \hbar \omega_{Lj}}$ , where  $\kappa_j$  is the decay rate of the cavity mode  $j$  and  $P_j$  is the power of the driving laser  $j$ . In the interaction picture, the Hamiltonian (1) can be written as

$$\begin{aligned}
 H = & \hbar (\delta_1 - \delta_{ab}) a_1^\dagger a_1 + \hbar (\delta_2 - \delta_{bc}) a_2^\dagger a_2 + \hbar \delta_1 \sigma_{aa} - \hbar \delta_2 \sigma_{cc} \\
 & + \frac{p^2}{2m} - \hbar g_1 a_1^\dagger a_1 \cos^2(k_1 x) - \hbar g_2 a_2^\dagger a_2 \cos^2(k_2 x - \varphi) \\
 & + \hbar (G_1 \sigma_{ba} a_1^\dagger + G_2 \sigma_{cb} a_2^\dagger + \text{H.c.}) + i \hbar (\varepsilon_1 a_1^\dagger - \varepsilon_1^* a_1) \\
 & + i \hbar (\varepsilon_2 a_2^\dagger - \varepsilon_2^* a_2), \quad (2)
 \end{aligned}$$

where  $\delta_{ab} = E_a - E_b - \omega_1$ ,  $\delta_{bc} = E_b - E_c - \omega_2$ ,  $\delta_1 = E_a - E_b - \omega_{L1}$ , and  $\delta_2 = E_b - E_c - \omega_{L2}$ . Thus,  $\delta_1 - \delta_{ab} = \omega_1 - \omega_{L1}$  ( $\delta_2 - \delta_{bc} = \omega_2 - \omega_{L2}$ ) denotes the detuning between the cavity field with frequency  $\omega_1$  ( $\omega_2$ ) and the classical driving field with frequency  $\omega_{L1}$  ( $\omega_{L2}$ ). With the fluctuation-dissipation processes affecting the optical fields,

the mechanical oscillator, and the atoms, the dynamics of the system is determined by the following Heisenberg-Langevin equations:

$$\dot{x} = p/m, \quad (3a)$$

$$\dot{p} = -\hbar g_1 k_1 a_1^\dagger a_1 \sin(2k_1 x) - \hbar g_2 k_2 a_2^\dagger a_2 \sin(2k_2 x - 2\varphi) \quad (3b)$$

$$- \gamma_M p + \xi(t) + \sqrt{\gamma_{m1}} F_{p1}(t) + \sqrt{\gamma_{m2}} F_{p2}(t), \quad (3c)$$

$$\dot{a}_1 = -[\kappa_1 + i(\delta_1 - \delta_{ab})]a_1 + i g_1 \cos^2(k_1 x) a_1 - i G_1 \sigma_{ba} \quad (3d)$$

$$+ \varepsilon_1 + \sqrt{2\kappa_1} a_{1,\text{in}}, \quad (3e)$$

$$\dot{a}_2 = -[\kappa_2 + i(\delta_2 - \delta_{bc})]a_2 + i g_2 \cos^2(k_2 x - \varphi) a_2$$

$$- i G_2 \sigma_{cb} + \varepsilon_2 + \sqrt{2\kappa_2} a_{2,\text{in}},$$

$$\dot{\sigma}_{ba} = -(\gamma + i\delta_1)\sigma_{ba} - i G_1 a_1 (\sigma_{bb} - \sigma_{aa}) + i G_2 a_2^\dagger \sigma_{ca}$$

$$+ \sqrt{2\gamma} c_{1,\text{in}},$$

$$\dot{\sigma}_{cb} = -(\gamma + i\delta_2)\sigma_{cb} - i G_1 a_1^\dagger \sigma_{ca} - i G_2 a_2 (\sigma_{cc} - \sigma_{bb})$$

$$+ \sqrt{2\gamma} c_{2,\text{in}}, \quad (3f)$$

where the overdots denote time derivatives.  $\xi(t)$  is the Brownian noise with zero mean value, which is characterized by the following correlation function [65]  $\langle \xi(t)\xi(t') \rangle = \frac{\hbar\gamma_M}{2\pi} \int d\omega e^{-i\omega(t-t')} \omega [1 + \coth(\frac{\hbar\omega}{2k_B T})]$ , where  $k_B$  is the Boltzmann constant and  $T$  is the temperature related to the nanosphere. In general, in the levitated optomechanical system placed in a high-vacuum chamber, a high mechanical quality factor can be attained for the optically trapped dielectric nanosphere and therefore the thermal damping rate  $\gamma_M$  is negligible [66,67]. In contrast, the diffusion rate ( $\gamma_{mj}$ ) of the levitated nanosphere caused by the photon recoil from the cavity fields should be included in the system dynamics, which can be estimated by  $\gamma_{mj} = \phi_j \omega_m$  with  $\phi_j = \frac{4\pi^2 V}{5\lambda_{Lj}^3} \frac{\epsilon-1}{\epsilon+2}$  [9].  $\lambda_{Lj}$  is the wavelength of the driving laser beam  $j$ . It should be noted that recoil heating effect does not contribute to any mechanical damping of the nanosphere, but only diffusion [68].  $F_{pj}(t)$  is the noisy force acting on the nanosphere due to photon recoil, which has the correlation [68]  $\langle F_{pj}(t)F_{pj}(t') \rangle = \delta(t-t')$ .  $a_{j,\text{in}}$  and  $c_{j,\text{in}}$  are the optical and atomic noise operators, respectively. They are fully characterized by the correlation functions,  $\langle a_{j,\text{in}}(t)a_{j,\text{in}}^\dagger(t') \rangle = \delta(t-t')$  and  $\langle c_{j,\text{in}}(t)c_{j,\text{in}}^\dagger(t') \rangle = \delta(t-t')$ .  $\gamma$  denotes the atomic decay.

In order to obtain the steady-state solution of the system, we use the linear approximation theory to solve the last two equations, (3) and (3) [69]. That is,  $\sigma_{i'i'}$  is substituted by  $\langle \sigma_{i'i'} \rangle$  for the terms containing  $\sigma_{i'i'} \times a_j$  or  $\sigma_{i'i'} \times a_j^\dagger$  so that the last two equations are expanded to the first order in  $G_j$  in Eq. (3). The approximation holds as long as the field operator changes slowly during the average lifetime of the atoms so that they can reach the steady state in a short time. This is because the states of the atoms and the cavity modes can be generally uncorrelated whether the atoms reside in or leave the cavity [49,69]. Further, we assume that the initial state of the atoms specified by the density  $\rho_a = \rho_{aa}^0 |a\rangle\langle a| + \rho_{cc}^0 |c\rangle\langle c| + \rho_{ca}^0 (|c\rangle\langle a| + |a\rangle\langle c|)$  and the atoms are injected into the cavity

at a normalized injection rate  $r_a$ . Consequently, the last two equations of Eq. (3) can be written as

$$\dot{\sigma}_{ba} = -(\gamma + i\delta_1)\sigma_{ba} + i G_1 r_a \rho_{aa}^0 a_1 + i G_2 r_a \rho_{ca}^0 a_2^\dagger + \sqrt{2\gamma} c_{1,\text{in}}, \quad (4a)$$

$$\dot{\sigma}_{cb} = -(\gamma + i\delta_2)\sigma_{cb} - i G_1 r_a \rho_{ca}^0 a_1^\dagger - i G_2 r_a \rho_{cc}^0 a_2 + \sqrt{2\gamma} c_{2,\text{in}}. \quad (4b)$$

By combining it with Eq. (3), the steady-state values of the hybrid system can be obtained by setting the time derivatives to zero, resulting in  $g_1 |a_{1s}|^2 k_1 \sin(2k_1 x_s) + g_2 |a_{2s}|^2 k_2 \sin(2k_2 x_s - 2\varphi) = 0$ ,  $p_s = 0$ ,  $a_{1s} = \frac{u_1^* \varepsilon_1 + u_1 \varepsilon_1^*}{u_1 u_2^* + u_{1a} u_{2c}^*}$ , and  $a_{2s} = \frac{u_1^* \varepsilon_2 - u_2 \varepsilon_1^*}{u_1^* u_2 + u_{2c} u_{1a}^*}$ , where  $u_j = \frac{G_1 G_2 r_a \rho_{ca}^0}{\gamma + i\delta_j}$  ( $j = 1, 2$ ),  $u_{1a} = \kappa_1 + i\Delta_1 - \frac{G_1^2 r_a \rho_{aa}^0}{\gamma + i\delta_1}$  with  $\Delta_1 = \delta_1 - \delta_{ab} - g_1 \cos^2(k_1 x_s)$ , and  $u_{2c} = \kappa_2 + i\Delta_2 + \frac{G_2^2 r_a \rho_{cc}^0}{\gamma + i\delta_2}$  with  $\Delta_2 = \delta_2 - \delta_{bc} - g_2 \cos^2(k_2 x_s - \varphi)$ . Clearly, the steady-state values of the hybrid system depend strongly on the parameters of the atomic medium, such as the initial population of the upper level  $\rho_{aa}^0$ , that of the lower level  $\rho_{cc}^0$ , and their coherence  $\rho_{ca}^0$ . Next we focus on the linearized dynamics of the quantum fluctuation around the semiclassical fixed points, in which the steady-state photon number in the cavity should be large, i.e.,  $\alpha_{1s} \gg 1$  and  $\alpha_{2s} \gg 1$ . In this case, one splits the operators in Eqs. (3) and (4) into their steady-state values and quantum fluctuations, e.g.,  $O = O_s + \delta O$  ( $O = x, p, a_1, a_2, \sigma_{ba}, \sigma_{cb}$ ). By inserting the ansatz  $O = O_s + \delta O$  into Eqs. (3) and (4) and neglecting all the terms higher than linear order in the fluctuation  $\delta O$ , the quantum Langevin equations for the fluctuations can be written as

$$\delta \dot{x} = \omega_m \delta p, \quad (5a)$$

$$\delta \dot{p} = -\omega_m \delta x - G_{p1} (a_{1s}^* \delta a_1 + a_{1s} \delta a_1^\dagger) - G_{p2} (a_{2s}^* \delta a_2 + a_{2s} \delta a_2^\dagger) + \sqrt{\gamma_{m1}} F_{p1}(t) + \sqrt{\gamma_{m2}} F_{p2}(t), \quad (5b)$$

$$\delta \dot{a}_1 = -(\kappa_1 + i\Delta_1) \delta a_1 - i G_{p1} a_{1s} \delta x - i G_1 \delta \sigma_{ba} + \sqrt{2\kappa_1} \delta a_{1,\text{in}}, \quad (5c)$$

$$\delta \dot{a}_2 = -(\kappa_2 + i\Delta_2) \delta a_2 - i G_{p2} a_{2s} \delta x - i G_2 \delta \sigma_{cb} + \sqrt{2\kappa_2} \delta a_{2,\text{in}}, \quad (5d)$$

$$\delta \dot{\sigma}_{ba} = -(\gamma + i\delta_1) \delta \sigma_{ba} + i G_1 r_a \rho_{aa}^0 \delta a_1 + i G_2 r_a \rho_{ca}^0 \delta a_2^\dagger + \sqrt{2\gamma} \delta c_{1,\text{in}}, \quad (5e)$$

$$\delta \dot{\sigma}_{cb} = -(\gamma + i\delta_2) \delta \sigma_{cb} - i G_2 r_a \rho_{cc}^0 \delta a_2 - i G_1 r_a \rho_{ca}^0 \delta a_1^\dagger + \sqrt{2\gamma} \delta c_{2,\text{in}}, \quad (5f)$$

where  $G_{p1} = \hbar g_1 k_1 \sin(2k_1 x_s) / \sqrt{\hbar m \omega_m}$  and  $G_{p2} = \hbar g_2 k_2 \sin(2k_2 x_s - 2\varphi) / \sqrt{\hbar m \omega_m}$  are the effective optomechanical coupling coefficients. The effective frequency  $\omega_m$  associated with c.m. oscillation of the levitated nanosphere is given as

$$\omega_m = \{2\hbar [g_1 k_1^2 |a_{1s}|^2 \cos(2k_1 x_s) + g_2 k_2^2 |a_{2s}|^2 \cos(2k_2 x_s - 2\varphi)] / m\}^{1/2}. \quad (6)$$

Here the position and momentum fluctuations  $\delta x$  and  $\delta p$  have been nondimensionalized as  $\sqrt{m \omega_m} / \hbar \delta x \rightarrow \delta x$  and

$\sqrt{1/\hbar m \omega_m} \delta p \rightarrow \delta p$  in Eq. (5). In addition, the thermal damping force  $\gamma_M \delta p$  in Eq. (5b) is neglected because  $\gamma_M$  is tiny.

Further, by introducing the column vector of the fluctuation operators  $f^T(t) = (\delta x, \delta p, \delta X_1, \delta Y_1, \delta X_2, \delta Y_2, \delta U_1, \delta V_1, \delta U_2, \delta V_2)$  and the corresponding noise vector  $n^T(t) = (0, \sqrt{\gamma_{m1}} F_{p1} + \sqrt{\gamma_{m2}} F_{p2}, \sqrt{2\kappa_1} \delta X_{1,\text{in}}, \sqrt{2\kappa_1} \delta Y_{1,\text{in}}, \sqrt{2\kappa_2} \delta X_{2,\text{in}}, \sqrt{2\kappa_2} \delta Y_{2,\text{in}}, \sqrt{2\gamma} \delta U_{1,\text{in}}, \sqrt{2\gamma} \delta V_{1,\text{in}}, \sqrt{2\gamma} \delta U_{2,\text{in}}, \sqrt{2\gamma} \delta V_{2,\text{in}})$ , where  $\delta X_j = (\delta a_j + \delta a_j^\dagger)/\sqrt{2}$ ,  $\delta Y_j = (\delta a_j - \delta a_j^\dagger)/\sqrt{2}i$ ,  $\delta U_1 = (\sigma_{ba} + \sigma_{ab})/\sqrt{2}$ ,  $\delta V_1 = (\sigma_{ba} - \sigma_{ab})/\sqrt{2}i$ ,  $\delta U_2 = (\sigma_{cb} +$

$\sigma_{bc})/\sqrt{2}$ , and  $\delta V_2 = (\sigma_{cb} - \sigma_{bc})/\sqrt{2}i$ ; the Hermitian input noise operators  $\delta X_{j,\text{in}} = (\delta a_{j,\text{in}} + \delta a_{j,\text{in}}^\dagger)/\sqrt{2}$ ,  $\delta Y_{j,\text{in}} = (\delta a_{j,\text{in}} - \delta a_{j,\text{in}}^\dagger)/\sqrt{2}i$ ,  $\delta U_{j,\text{in}} = (\delta c_{j,\text{in}} + \delta c_{j,\text{in}}^\dagger)/\sqrt{2}$ , and  $\delta V_{j,\text{in}} = (\delta c_{j,\text{in}} - \delta c_{j,\text{in}}^\dagger)/\sqrt{2}i$ , the set of linear quantum Langevin equations can be written in the following matrix form

$$\dot{f}(t) = Af(t) + n(t). \quad (7)$$

Here  $A$  is the  $10 \times 10$  drift matrix, given by

$$A = \begin{pmatrix} 0 & \omega_m & 0 & 0 & 0 & 0 & 0 & 0 & 0 & 0 \\ -\omega_m & 0 & -G_{p1}X_{1s} & -G_{p1}Y_{1s} & -G_{p2}X_{2s} & -G_{p2}Y_{2s} & 0 & 0 & 0 & 0 \\ G_{p1}Y_{1s} & 0 & -\kappa_1 & \Delta_1 & 0 & 0 & 0 & G_1 & 0 & 0 \\ -G_{p1}X_{1s} & 0 & -\Delta_1 & -\kappa_1 & 0 & 0 & -G_1 & 0 & 0 & 0 \\ G_{p2}Y_{2s} & 0 & 0 & 0 & -\kappa_2 & \Delta_2 & 0 & 0 & 0 & G_2 \\ -G_{p2}X_{2s} & 0 & 0 & 0 & -\Delta_2 & -\kappa_2 & 0 & 0 & -G_2 & 0 \\ 0 & 0 & 0 & -G_1 r_a \rho_{aa}^0 & 0 & G_2 r_a \rho_{ca}^0 & -\gamma & \delta_1 & 0 & 0 \\ 0 & 0 & G_1 r_a \rho_{aa}^0 & 0 & G_2 r_a \rho_{ca}^0 & 0 & -\delta_1 & -\gamma & 0 & 0 \\ 0 & 0 & 0 & -G_1 r_a \rho_{ca}^0 & 0 & G_2 r_a \rho_{cc}^0 & 0 & 0 & -\gamma & \delta_2 \\ 0 & 0 & -G_1 r_a \rho_{ca}^0 & 0 & -G_2 r_a \rho_{cc}^0 & 0 & 0 & -\delta_2 & -\gamma & 0 \end{pmatrix}, \quad (8)$$

where  $X_{js} = (a_{js}^* + a_{js})/\sqrt{2}$  and  $Y_{js} = (a_{js} - a_{js}^*)/\sqrt{2}i$ .

The steady state of the hybrid system is unique when the solutions to Eq. (5) are stable, i.e., the real parts of all eigenvalues of the matrix  $A$  are negative. The stability condition can be formulated by using the Routh-Hurwitz criteria [70]. In spite of this fact, the explicit inequalities are quite cumbersome. Here, we check the stability of the steady-state solutions with numerical calculation to ensure that the parameters we used always satisfy the stability conditions.

The nature of linear quantum correlations among the cavity fields and the nanosphere can be investigated by the correlation matrix ( $V$ ) of quantum fluctuations in the hybrid system, whose element can be defined as  $V_{ij} = \langle f_i(\infty) f_j(\infty) + f_j(\infty) f_i(\infty) \rangle / 2$  because the steady state of the present system is always a zero-mean multipartite Gaussian state. Further, we can solve the linearized Langevin equation (7) for the fluctuations to obtain the steady-state correlation matrix that satisfies the following Lyapunov equation [30]:

$$AV + VA^T = -D, \quad (9)$$

where  $D = \text{diag}[0, (\gamma_{m1} + \gamma_{m2})/2, \kappa_1, \kappa_1, \kappa_2, \kappa_2, \gamma, \gamma, \gamma, \gamma]$ . In order to study the optomechanical entanglement in the system and the influence of the three-level atoms, we consider the bipartite entanglement between the levitated nanosphere and the cavity mode 1 or 2. The bipartite subsystem can be formed by tracing over the remaining degrees of freedom and such bipartite entanglement is quantified by using the logarithmic negativity,  $E_N$ , and given by [71]

$$E_N = \max[0, -\ln 2\nu_{\min}], \quad (10)$$

where  $\nu_{\min}$  is the smallest symplectic eigenvalue of the partially transposed correlation matrix associated with the selected bipartite subsystem. The corresponding reduced cor-

relation matrix can be represented in a  $2 \times 2$  block form  $V_{bp} = \begin{pmatrix} A_1 & C \\ C^T & A_2 \end{pmatrix}$ , obtained by neglecting the columns and rows of uninteresting modes in the  $10 \times 10$  correlation matrix  $V$ . For example, when the bipartite entanglement  $E_{N1}$  between the nanosphere and the cavity mode 1 is evaluated, we have  $A_1 = \begin{pmatrix} V_{11} & V_{12} \\ V_{21} & V_{22} \end{pmatrix}$ ,  $A_2 = \begin{pmatrix} V_{33} & V_{34} \\ V_{43} & V_{44} \end{pmatrix}$ , and  $C = \begin{pmatrix} V_{13} & V_{14} \\ V_{23} & V_{24} \end{pmatrix}$ . In this manner, the smallest symplectic eigenvalue is  $\nu_{\min} = 2^{-1/2} [\Sigma - \sqrt{\Sigma - 4 \det V_{bp}}]^{1/2}$  with  $\Sigma = \det A_1 + \det A_2 - 2 \det C$ . The block matrix for the bipartite subsystem of the nanosphere and the cavity mode 2 and the corresponding bipartite entanglement  $E_{N2}$  can be obtained similarly.

### III. NUMERICAL RESULTS

In general, the generation of the entanglement between the mechanical and the optical modes results from the coupling between them, which can be controlled coherently with a proper design of the atomic state [49]. In this section, we evaluate in detail the entanglement between the levitated nanosphere and the cavity modes in the presence of the injected atomic medium. For simplicity, in the numerical calculations, we assumed that the two cavity modes 1 and 2 have similar properties, i.e.,  $\omega_1 \approx \omega_2 = \omega_c$ ,  $\kappa_1 \approx \kappa_2 = \kappa$ , etc. However, we stress that in the present hybrid optomechanical system, the photons of different modes should be distinguished and driven separately by the external driving lasers with different frequencies  $\omega_{L1}$  and  $\omega_{L2}$ . This is possible when the frequency difference between the modes 1 and 2,  $|\omega_1 - \omega_2|$ , is much larger than the decay rates of the photons and the oscillation frequency of the levitated nanosphere, both of which are only in the order of 1 MHz [64]. This means that the previous numerical assumption, i.e.,  $\omega_1 \approx \omega_2$ , is not contradictory to the two-mode driving setup. Further,

we choose that the wavelength of driving laser field 1 and the cavity decay rate are  $\lambda_{L1} = 810$  nm and  $\kappa_1 = 0.2$  MHz, respectively. In order to evaluate the coupling between the levitated nanosphere and the cavity modes, we take the radius of the silicon nanosphere  $r = 100$  nm with the dielectric constant  $\epsilon = 2$  and the density  $\rho = 2300$  kg/m<sup>3</sup>. The silicon nanosphere is used for its stability near the high melting point and the high polarizability-to-mass ratio, which was successfully done in experiments [13]. The length of the cavity and the mode waist are  $L = 3$  mm and  $w_j = 25$   $\mu$ m, respectively; the corresponding mode volume can be evaluated as  $V_{cj} = (\pi/4)Lw_j^2$ . In addition, the driving power of the laser is relatively small, i.e.,  $P = P_1 = 20$   $\mu$ W, which ensures that the nanosphere will not be melted. We further take the phase  $\varphi = \pi/12$  and consider laser field 1 driving with a slightly larger power than field 2, with a ratio  $R = \epsilon_2/\epsilon_1 = 0.8$ .

The other parameter, i.e., the initial state of the atomic medium injected into the cavity, is assumed to be  $|\psi_A(0)\rangle = C_a|a\rangle + C_c|c\rangle$ . That is, there is no population in the intermediate level  $|b\rangle$ . In this case, the initial density matrix is calculated as  $\rho_a(0) = |\psi_A\rangle\langle\psi_A| = \rho_{aa}^0|a\rangle\langle a| + \rho_{cc}^0|c\rangle\langle c| + (\rho_{ca}^0|c\rangle\langle a| + \text{H.c.})$ , where  $\rho_{aa}^0 = |C_a|^2$  and  $\rho_{cc}^0 = |C_c|^2$  are the initial populations of the upper and lower levels, respectively;  $\rho_{ca}^0 = C_a^*C_c$  describes the initial two-photon atomic coherence; and the two optical fields  $a_1$  and  $a_2$  will be correlated when  $\rho_{ca}^0 \neq 0$ . In order to investigate the impact of the atomic coherence on the steady-state optomechanical entanglement, we introduced a new coherent superposition parameter  $\eta \in [-1, 1]$  to characterize the initial atomic medium, i.e.,  $\rho_{aa}^0 = (1 - \eta)/2$  and  $\rho_{cc}^0 = (1 + \eta)/2$ , and the corresponding atomic coherence, i.e.,  $\rho_{ca}^0 = \sqrt{1 - \eta^2}/2$  [50]. It is easy to find that  $\rho_{aa}^0$  ( $\rho_{cc}^0$ ) decreases (increases) with the increase of  $\eta$ . In contrast, the atomic coherence  $\rho_{ca}^0$  increases first and then decreases to 0 with the increase of  $\eta$ . The optimal coherence of the atomic initial state can be attained when  $\eta = 0$ . The atomic detunings  $\delta_1 = \delta_2 = \pi$  MHz, the decay rate  $\gamma = 2$  MHz, the atom-field couplings  $G_1 = G_2 = 1.6\pi \times 10^3$  Hz, and the normalized injection rate  $r_a = 2000$ . In Fig. 2, we consider the dependence of the oscillation frequency of the nanosphere on the effective cavity field detunings  $\Delta_1$  and  $\Delta_2$  with  $\eta = 0.6$  and the corresponding atomic coherence  $\rho_{ca}^0 = 0.4$ . It can be seen that the frequency of the levitated nanosphere depends strongly on the effective detunings  $\Delta_1$  and  $\Delta_2$ . In particular, in the case of small detunings  $\Delta_1$  and  $\Delta_2$ , there is always a relatively large oscillation frequency, which comes from two terms: the contribution of the cavity field 1 plus that from cavity field 2 [see Eq. (6)]. Clearly, the two contributions are proportional to the intracavity mean photon number, i.e.,  $|\alpha_{1s}|^2$  or  $|\alpha_{2s}|^2$ , which increases with the decreasing moduli of the effective detuning  $\Delta_1$  or  $\Delta_2$ .

Figures 3(a) and 3(b) show the bipartite entanglement between the levitated nanosphere and the cavity modes in the steady state,  $E_{N1}$  and  $E_{N2}$ , as a function of the positive effective detunings  $\Delta_1$  and  $\Delta_2$ . It is clear from Fig. 3 that the entanglement can appear in the positive detuning region. Further, the entanglement between the nanosphere and the cavity mode 1 reaches a maximum  $E_{N1}^{\max} = 0.054$  at  $\Delta_1^{\max} = 2.8\kappa$  and  $\Delta_2^{\max} = 2.3\kappa$ . The corresponding effective oscillation frequency of the nanosphere is  $\omega_m = 2.63\kappa$  (see Fig. 2), which

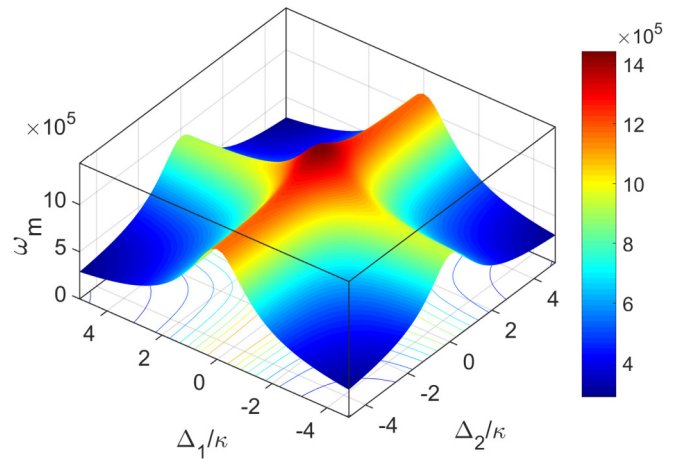


FIG. 2. Plot of the oscillating frequency of the dielectric nanosphere,  $\omega_m$ , as a function of the effective cavity field detunings  $\Delta_1$  and  $\Delta_2$ . We assume that the atoms are prepared in coherent superposition state with  $\eta = 0.6$ . We have taken the modes 1 and 2 with similar properties, i.e.,  $\omega_1 \approx \omega_2 = \omega_c$ ,  $\kappa_1 \approx \kappa_2 = \kappa$ , etc. The wavelength of laser field 1 is  $\lambda_{L1} = 810$  nm, the driving power  $P_1 = 20$   $\mu$ W, and the cavity decay rate  $\kappa_1 = 0.2$  MHz. We have taken  $\varphi = \pi/12$  and laser field 1 has a slightly larger power than laser field 2, i.e.,  $R = 0.8$ . The other parameters are the atomic detunings  $\delta_1 = \delta_2 = \pi$  MHz, normalized injection rate  $r_a = 2000$ , atom-field couplings  $G_1 = G_2 = 1.6\pi \times 10^3$  Hz, and decay rate  $\gamma = 2$  MHz; the radius of silica nanosphere  $r = 100$  nm, density  $\rho = 2300$  kg/m<sup>3</sup>, and dielectric constant  $\epsilon = 2$ ; and the cavity length  $L = 3$  mm and mode waist  $w = 25$   $\mu$  m.

approaches the optimal detuning  $\Delta_1^{\max}$ . It displays an optimal cooling in cavity field 1 due to the beam-splitter interaction and therefore leads to a maximal entanglement. When the effective cavity field detunings  $\Delta_1$  and  $\Delta_2$  are far away from the effective oscillation frequency, the log negativities,  $E_{N1}$  and  $E_{N2}$ , decrease gradually to 0 and therefore the optomechanical entanglement disappears. For the nanosphere and cavity mode 2, the entanglement maximum is  $E_{N2}^{\max} = 0.105$  for  $\Delta_1^{\max} = 2.6\kappa$  and  $\Delta_2^{\max} = 2.4\kappa$ , which shows up in the resonance region with  $\omega_m \approx \Delta_1^{\max}$ , corresponding to an optimal cooling of the cavity field. It is found from Figs. 3(a) and 3(b) that due to the fact that the effective optomechanical coupling strength  $|G_{p2}a_{2s}| > |G_{p1}a_{1s}|$ , the maximum entanglement  $E_{N2}^{\max}$  is larger than  $E_{N1}^{\max}$ , which reveals the role of the optomechanical interaction in the generation of entanglement.

In addition, it is noted that the two-mode squeezing interactions arising from the mechanical blue-sideband driving may enhance the optomechanical entanglement. Therefore, we consider the case that the one of the cavity field detuning is negative, i.e.,  $\Delta_1 < 0$ , and study the generation of entanglement. In Fig. 4, we show the bipartite entanglement,  $E_{N1}$  and  $E_{N2}$ , as a function of the negative detuning  $\Delta_1$  and the positive one  $\Delta_2$ . We can see from Fig. 4(a) that the maximum entanglement  $E_{N1}^{\max} = 0.237$  can be obtained due to the two-mode squeezing interaction when  $\Delta_1 = -2.6\kappa$ , which is larger than that under the mechanical red-sideband driving, i.e.,  $\Delta_1 > 0$ . In contrast, it is found from Fig. 4(b) that the entanglement between the levitated nanosphere and cavity field 2 declines due to the dominating role of the blue-detuning mode 1. We

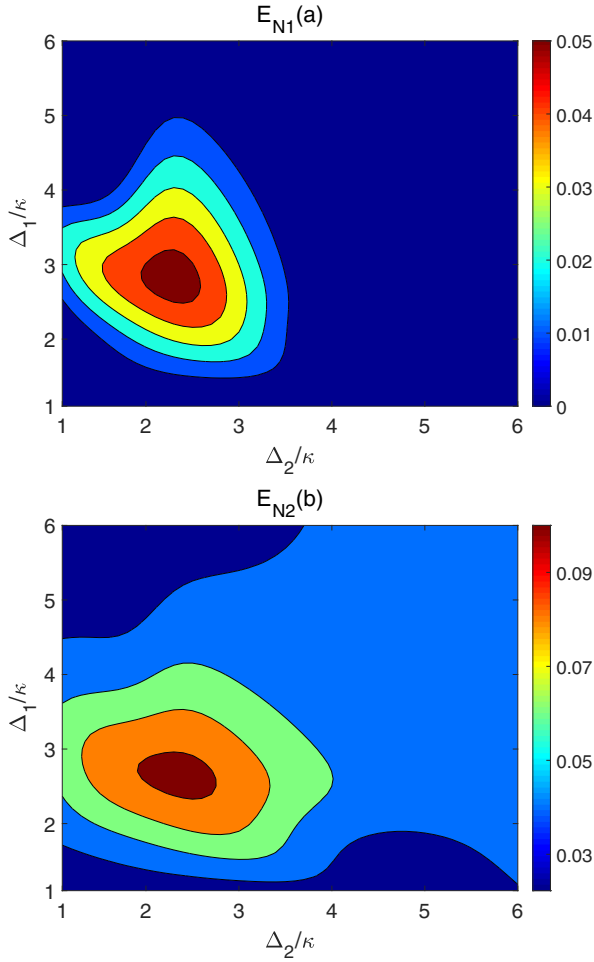


FIG. 3. Plot of the entanglements,  $E_{N1}$  (a) and  $E_{N2}$  (b), as a function of the effective positive detunings  $\Delta_1$  and  $\Delta_2$ . Other parameter values are the same as in Fig. 2.

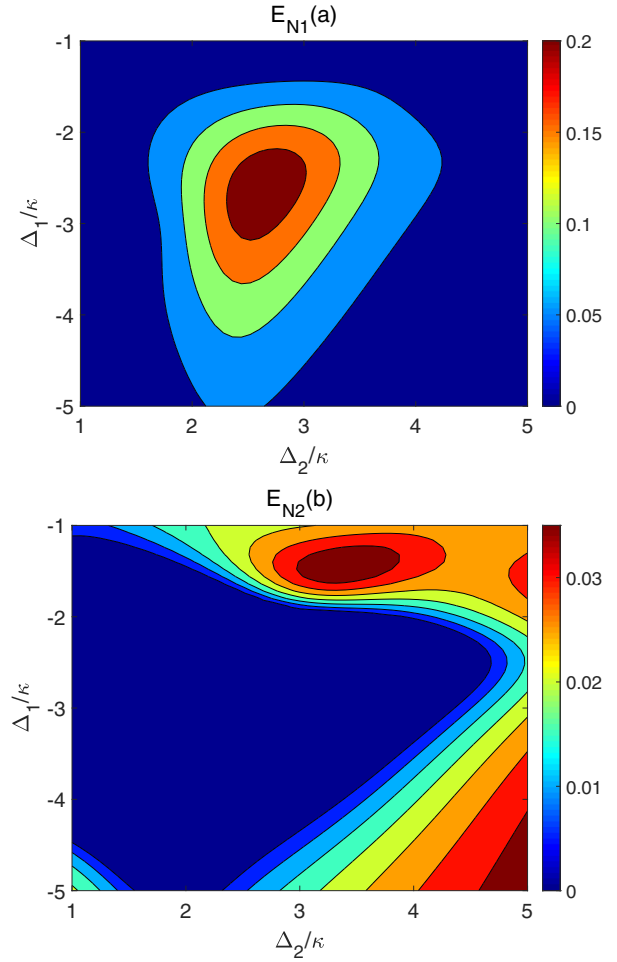


FIG. 4. Plot of the entanglements,  $E_{N1}$  (a) and  $E_{N2}$  (b), as a function of the effective negative detuning  $\Delta_1$  and the positive detuning  $\Delta_2$ . Other parameter values are the same as in Fig. 2.

also evaluate the stability of the system by considering the maximum eigenvalue of the drift matrix  $A$ . Figure 5 shows the maximum eigenvalue as a function of the effective detunings  $\Delta_1$  and  $\Delta_2$ . It is found from Fig. 5 that the optimal entanglements in Figs. 3 and 4 appear in the stable region of the system.

Next, we investigate the role of the atomic coherent superposition in the generation of the steady-state entanglement near the optimal cavity field detunings. Figure 6 shows the bipartite entanglement,  $E_{N1}$  and  $E_{N2}$ , as a function of atom-field coupling strength  $G$  with different  $\eta$ . The driving power is  $P = P_1 = 50 \mu\text{W}$  and the optimal cavity detunings  $\Delta_1 = \Delta_2 \approx 3\kappa$ . Other parameter values are the same as in Fig. 2. It is found from Fig. 6(a) that when the atomic coherence is fixed, i.e.,  $\rho_{ca}^0 = 0.4$ , the coherent superposition parameter  $\eta$  is 0.6 or  $-0.6$  and therefore these exist two different values of the bipartite entanglement  $E_{N1}$ . Similar characteristics appear for the bipartite entanglement  $E_{N2}$ ; see Fig. 6(b). This means that the optomechanical entanglement in the hybrid system is sensitive to the initial population of the atomic states, which affects significantly the effective optomechanical coupling. Furthermore, when the atomic population is changed from the upper level to the lower level, the bipartite entanglements  $E_{N1}$

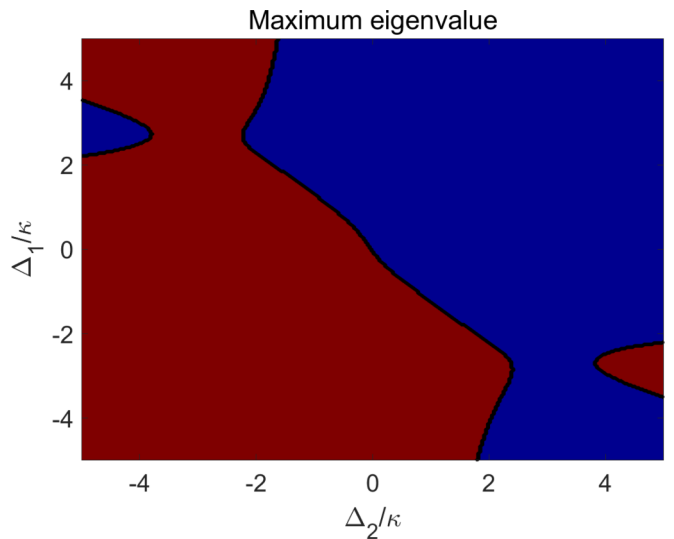


FIG. 5. Plot of the maximum eigenvalue of the drift matrix  $A$  as a function of the effective detunings  $\Delta_1$  and  $\Delta_2$ . The blue region denotes that the maximum eigenvalue of the drift matrix  $A$  is negative and therefore the system is stable. The parameter values are the same as in Fig. 2.

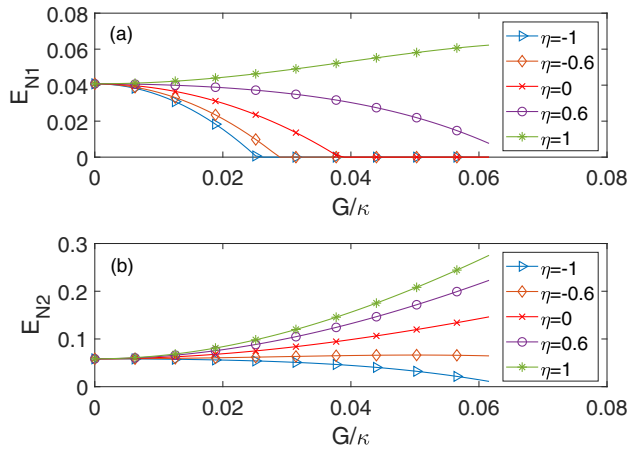


FIG. 6. Plot of the entanglements,  $E_{N1}$  (a) and  $E_{N2}$  (b), as functions of the atom-field coupling strength  $G$  with different  $\eta$ . The driving power  $P = P_1 = 50 \mu\text{W}$  and the optimal cavity detunings  $\Delta_1 = \Delta_2 = 3\kappa$ . The effective atom-field couplings are assumed to be equal, i.e.,  $G_1 = G_2 = G$ . Other parameter values are the same as in Fig. 2.

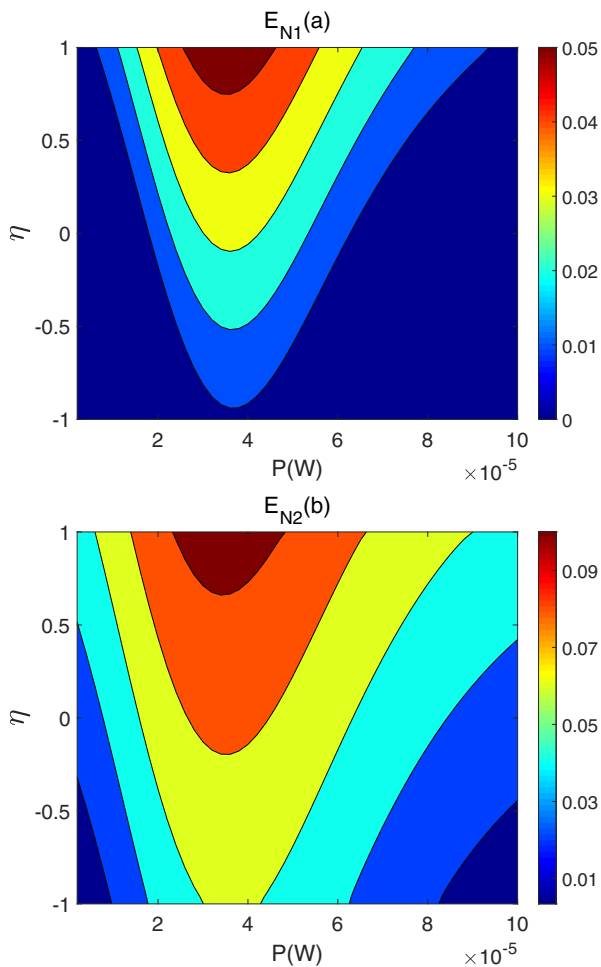


FIG. 7. Plot of the entanglements,  $E_{N1}$  (a) and  $E_{N2}$  (b), as functions of the driving power  $P$  and the coherent superposition  $\eta$ . Other parameters are the same as in Fig. 6.

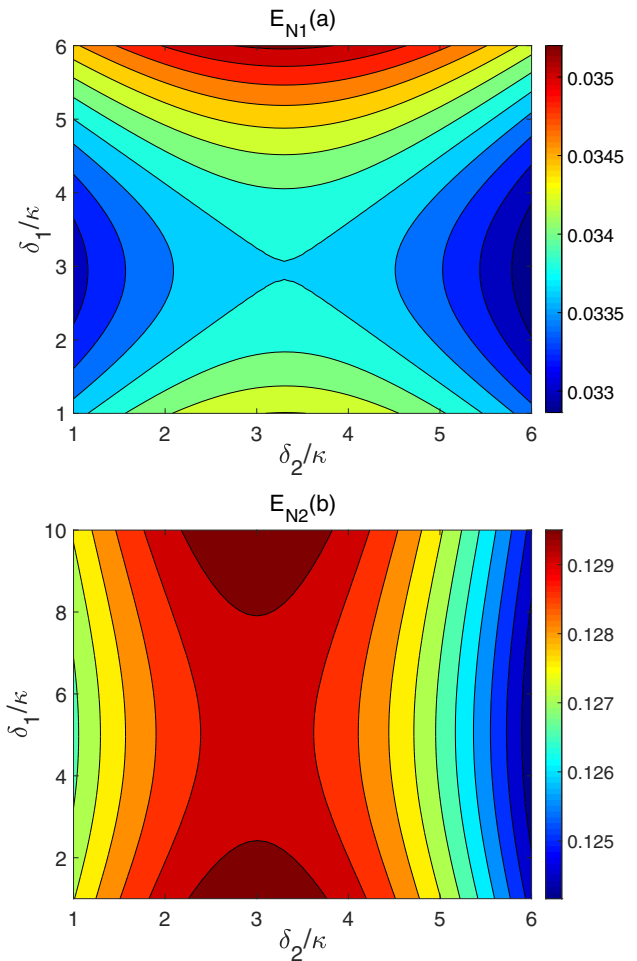


FIG. 8. Plot of the entanglements,  $E_{N1}$  (a) and  $E_{N2}$  (b), as functions of the atomic detunings  $\delta_1$  and  $\delta_2$ . Other parameters are the same as in Fig. 6.

and  $E_{N2}$  increase monotonically. The entanglement maximum appears at  $\eta = 1$  and  $\rho_{ca} = 0$ . Therefore, the large initial population of lower level  $|c\rangle$  can enhance the optomechanical entanglement. In addition, we can see from Fig. 6 that the bipartite entanglements  $E_{N1}$  and  $E_{N2}$  decrease with the increase of  $G$  if all atoms are initially in the upper level, i.e., ( $\eta = -1$ ). In contrast, when the atoms are initially in the lower atomic level, i.e., ( $\eta = 1$ ), the bipartite entanglements  $E_{N1}$  and  $E_{N2}$  increase with the increase of  $G$ . Consequently, the injected atomic medium should be prepared initially in the lower level at a fixed atomic coherence  $\rho_{ca}^0$  to attain a large entanglement.

Figure 7 depicts  $E_{N1}$  and  $E_{N2}$  ( $\Delta_1 = \Delta_2 = 3\kappa$ ) as functions of the driving power  $P$  and the coherent superposition  $\eta$ . Clearly, we see from Figs. 7(a) and 7(b) that the maximum entanglements  $E_{N1}^{\max}$  and  $E_{N2}^{\max}$  always appear when the atoms are prepared in the lower level, i.e.,  $\eta = 1$ . Moreover, it is observed from Fig. 7 that the entanglements are not monotonic functions of the driving power  $P$  and that their maximums appear at certain intermediate values of  $P$  for different coherent superpositions  $\eta$ . In the present model, the increase of the driving power leads to large photon numbers  $|a_{1s}|^2$  and  $|a_{2s}|^2$ . Correspondingly, the effective oscillation frequency  $\omega_m$  of the

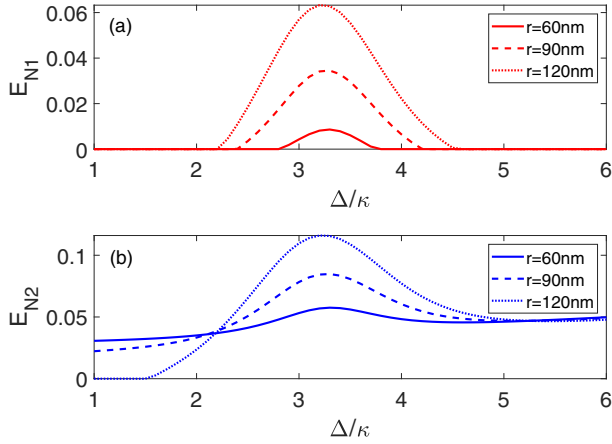


FIG. 9. Plot of the entanglements,  $E_{N1}$  (a) and  $E_{N2}$  (b), as functions of the effective cavity field detuning  $\Delta$  with different radius  $r$ . Here we take  $\Delta_1 = \Delta_2 = \Delta$ . Other parameters are the same as in Fig. 6.

levitated nanosphere becomes large gradually. Then, when the driving power of the system is relatively small or large,  $\omega_m$  will be very different from the effective cavity field detunings  $\Delta_1$  and  $\Delta_2$  so that the resonant coupling cannot be achieved, which leads to a small optomechanical entanglement.

In Fig. 8, we investigate the dependence of the optomechanical entanglements,  $E_{N1}$  and  $E_{N2}$ , upon the atomic detunings  $\delta_1$  and  $\delta_2$  near the optimal effective cavity field detunings with  $\Delta_1 = \Delta_2 = 3\kappa$ . In Fig. 8, the entanglements are not a monotonic function of the atomic detunings  $\delta_1$  and  $\delta_2$ . Further, for a given atomic detuning  $\delta_1$ , the maximum entanglement  $E_{N1}^{\max}$  appears in the region of  $\delta_2 \approx \Delta_2$ . In contrast, when the atomic detuning  $\delta_2$  is fixed, the bipartite entanglement  $E_{N1}$  decreases first and then increases with the increase of the atomic detuning  $\delta_1$  and the minimum  $E_{N1}^{\min}$  is attained at  $\delta_1 \approx \Delta_1$ . Similar characteristics are observed for the bipartite entanglement  $E_{N2}$  shown in Fig. 8(b). The results suggest that one should carefully choose the atomic detunings, which impact significantly the optomechanical entanglement and its maximum.

It was noted that increasing the radius of the nanosphere will enhance the optomechanical coupling  $g_j$  and therefore may help generate the steady-state optomechanical entanglement. Figures 9(a) and 9(b) portray the steady-state entanglements between the nanosphere and the cavity modes as functions of the dimensionless effective cavity field detuning  $\Delta/\kappa$  with different radius  $r$ , where we assume  $\Delta_1 = \Delta_2 = \Delta$ . Other parameters are the same as those in Fig. 6. In Fig. 9, we see clearly that in the resonant region with  $\Delta \approx \omega_m$ , the optomechanical entanglement in the steady state always increases with the radius of the nanosphere. In particular, the range of the effective cavity field detuning expands with the radius of the nanosphere. We stress that the radius of the nanosphere cannot increase too much because the recoil diffusion resulting from the cavity fields and the difficulty of levitating a heavy nanosphere.

Finally, it would be interesting to check the presence of genuine tripartite entanglement between the three degrees of

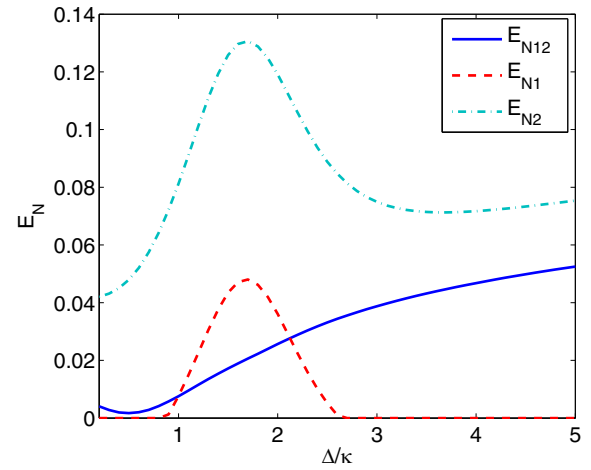


FIG. 10. Plot of the optomechanical entanglements,  $E_{N1}$  and  $E_{N2}$ , and the entanglement between the optical modes,  $E_{N12}$ , as functions of the effective cavity field detuning  $\Delta$  with  $\Delta_1 = \Delta_2 = \Delta$ . Here we have taken  $\delta_1 = \delta_2 = 6\pi \times 10^5$  Hz and  $P = 0.05 \times 10^{-4}$  W. Other parameters are the same as in Fig. 6.

freedom in the system, signaled by a simultaneous presence of bipartite entanglement across all three bipartitions [38–41,71]. For example, denoting  $E_{N12}$  as the residual entanglement between the two optical modes, then  $E_{N1}$ ,  $E_{N2}$ , and  $E_{N12}$  are all larger than zero, which means that the levitated nanosphere and the two cavity modes 1 and 2 are genuinely entangled with each other [38,71]. Figure 10 portrays the evolution of entanglement among the nanosphere and the two cavity fields as a function of the dimensionless effective cavity field detuning  $\Delta/\kappa$ , where we assume  $\Delta_1 = \Delta_2 = \Delta$ .  $\delta_1 = \delta_2 = 6\pi \times 10^5$  Hz and  $P = 0.05 \times 10^{-4}$  W. Other parameters are the same as those in Fig. 6. In Fig. 10, we see clearly that the simultaneous presence of bipartite entanglement across all three bipartitions, i.e.,  $E_{N1} > 0$ ,  $E_{N2} > 0$ , and  $E_{N12} > 0$ , appears in the intermediate region of the cavity field detuning  $\Delta$  so that the genuine multipartite entanglement between the two optical fields and the levitated nanosphere can be obtained by selecting the system's parameters properly. As a result, the present optomechanical system has potential applications in the generation of the bipartite and tripartite optomechanical entanglement, which may be useful for quantum information processing.

#### IV. CONCLUSIONS

In conclusion, we have analyzed a hybrid optomechanical system consisting of a Fabry-Pérot cavity with a three-level atomic medium and a levitated dielectric nanosphere, which are coupled with two driven cavity modes. We focused on the linearized dynamics around the semiclassical fixed point and discussed the steady-state optomechanical entanglement between the levitated nanosphere and the driven optical modes as a function of the control parameters of the cavity field, the atomic medium, and the nanosphere, which we found depend strongly on the initial population in different atomic states and the atomic detuning. Further, we showed the existence of the optimal effective cavity field detuning and the



driving power that maximize the optomechanical entanglement. We also investigated in detail the role of the radius of the nanosphere in the steady-state optomechanical entanglement and the generation of genuine tripartite entanglement between the three degrees of freedom in the system. The present study demonstrates that the atomic medium with a cascade configuration emerges as a flexible handle to coherently control the dynamics of the levitated nanosphere and hence provides a useful way to manipulate macroscopic quantum properties.

## ACKNOWLEDGMENTS

W.J.N. is supported by the National Natural Science Foundation of China (NSFC) under Grant No. 12065008, the Key Project of Youth Science Foundation of Jiangxi Province under Grant No. 20192ACBL21001, and the Natural Science Foundation of Jiangxi Province under Grant No. 20192BCBL23007. A.X.C. is supported by the NSFC under Grant No. 11775190. Y.H.L. is supported by the NSFC under Grant No. 11775035. Q.H.L. is supported by the NSFC under Grant No. 62061028.

- 
- [1] M. Aspelmeyer, T. J. Kippenberg, and F. Marquardt, *Rev. Mod. Phys.* **86**, 1391 (2014).
- [2] S. Weis, R. Rivière, S. Deléglise, E. Gavartin, O. Arcizet, A. Schliesser, and T. J. Kippenberg, *Science* **330**, 1520 (2010).
- [3] H. Xiong, L. Si, X. Y. Lü, X. Yang, and Y. Wu, *Sci. China: Phys., Mech. Astron.* **58**, 1 (2015).
- [4] F. Marquardt, J. G. E. Harris, and S. M. Girvin, *Phys. Rev. Lett.* **96**, 103901 (2006).
- [5] R. Ghobadi, A. R. Bahrapour, and C. Simon, *Phys. Rev. A* **84**, 033846 (2011).
- [6] M. Bhattacharya and P. Meystre, *Phys. Rev. Lett.* **99**, 073601 (2007).
- [7] Y. Li, L.-A. Wu, and Z. D. Wang, *Phys. Rev. A* **83**, 043804 (2011).
- [8] J. D. Thompson, B. M. Zwickl, A. M. Jayich, F. Marquardt, S. M. Girvin, and J. G. E. Harris, *Nature (London)* **452**, 72 (2008).
- [9] D. E. Chang, C. A. Regal, S. B. Papp, D. J. Wilson, J. Ye, O. Painter, H. J. Kimble, and P. Zoller, *Proc. Natl. Acad. Sci. USA* **107**, 1005 (2010).
- [10] Z.-Q. Yin, T. Li, and M. Feng, *Phys. Rev. A* **83**, 013816 (2011).
- [11] Z.-Q. Yin, A. A. Geraci, and T. C. Li, *Int. J. Mod. Phys. B* **27**, 1330018 (2013).
- [12] Z. Xu and T. Li, *Phys. Rev. A* **96**, 033843 (2017).
- [13] P. Asenbaum, S. Kuhn, S. Nimmrichter, U. Sezer, and M. Arndt, *Nat. Commun.* **4**, 2743 (2013).
- [14] J. D. Teufel, D. Donner, T. and Li, J. W. Harlow, M. S. Allman, K. Cicak, A. J. Sirois, J. D. Whittaker, K. W. Lehnert, and R. W. Simmonds, *Nature (London)* **475**, 359 (2011).
- [15] A. G. Krause, M. Winger, T. D. Blasius, Q. Lin, and O. Painter, *Nat. Photon.* **6**, 768 (2012).
- [16] J.-Q. Zhang, Y. Li, M. Feng, and Y. Xu, *Phys. Rev. A* **86**, 053806 (2012).
- [17] A. M. Armani, R. P. Kulkarni, S. E. Fraser, R. C. Flagan, and K. J. Vahala, *Science* **317**, 783 (2007).
- [18] A. Buonanno and Y. Chen, *Phys. Rev. D* **67**, 062002 (2003).
- [19] L. Conti, M. De Rosa, F. Marin, L. Taffarello, and M. Cerdonio, *J. Appl. Phys.* **93**, 3589 (2003).
- [20] P. Rab, *Phys. Rev. Lett.* **107**, 063601 (2011).
- [21] A. Pontin, M. Bonaldi, A. Borrielli, L. Marconi, F. Marino, G. Pandraud, G. A. Prodi, P. M. Sarro, E. Serra, and F. Marin, *Phys. Rev. Lett.* **116**, 103601 (2016).
- [22] W. K. Hensinger, D. W. Utami, H.-S. Goan, K. Schwab, C. Monroe, and G. J. Milburn, *Phys. Rev. A* **72**, 041405(R) (2005).
- [23] I. Wilson-Rae, N. Nooshi, W. Zwerger, and T. J. Kippenberg, *Phys. Rev. Lett.* **99**, 093901 (2007).
- [24] Y. Guo, K. Li, W. Nie, and Y. Li, *Phys. Rev. A* **90**, 053841 (2014).
- [25] W. Zeng, W. Nie, L. Li, and A. Chen, *Sci. Rep.* **7**, 17258 (2017).
- [26] W. Nie, A. Chen, and Y. Lan, *Opt. Express* **23**, 30970 (2015).
- [27] Y. C. Liu, Y. F. Xiao, X. Luan, Q. Gong, and C. W. Wong, *Phys. Rev. A* **91**, 033818 (2015).
- [28] Q. Zheng, J. Xu, Y. Yao, and Y. Li, *Phys. Rev. A* **94**, 052314 (2016).
- [29] G. Li, W. Nie, X. Li, M. Li, A. Chen, and Y. Lan, *Sci. China: Phys., Mech. Astron.* **62**, 100311 (2019).
- [30] D. Vitali, S. Gigan, A. Ferreira, H. R. Böhm, P. Tombesi, A. Guerreiro, V. Vedral, A. Zeilinger, and M. Aspelmeyer, *Phys. Rev. Lett.* **98**, 030405 (2007).
- [31] S. G. Hofer, W. Wieczorek, M. Aspelmeyer, and K. Hammerer, *Phys. Rev. A* **84**, 052327 (2011).
- [32] C. Genes, A. Mari, P. Tombesi, and D. Vitali, *Phys. Rev. A* **78**, 032316 (2008).
- [33] M. J. Hartmann and M. B. Plenio, *Phys. Rev. Lett.* **101**, 200503 (2008).
- [34] R. Ghobadi, S. Kumar, B. Pepper, D. Bouwmeester, A. I. Lvovsky, and C. Simon, *Phys. Rev. Lett.* **112**, 080503 (2014).
- [35] Y. D. Wang and A. A. Clerk, *Phys. Rev. Lett.* **110**, 253601 (2013).
- [36] M. Gao, F. Lei, C. Du, and G. Long, *Sci. China: Phys., Mech. Astron.* **59**, 610301 (2016).
- [37] G. Li, W. Nie, X. Li, and A. Chen, *Phys. Rev. A* **100**, 063805 (2019).
- [38] X. H. Yang, Y. Ling, X. Shao, and M. Xiao, *Phys. Rev. A* **95**, 052303 (2017).
- [39] G. De Chiara, M. Paternostro, and G. M. Palma, *Phys. Rev. A* **83**, 052324 (2011).
- [40] A. Xuereb, M. Barbieri, and M. Paternostro, *Phys. Rev. A* **86**, 013809 (2012).
- [41] B. Rogers, M. Paternostro, G. M. Palma, and G. De Chiara, *Phys. Rev. A* **86**, 042323 (2012).
- [42] R. Ikuta, T. Kobayashi, T. Kawakami, S. Miki, M. Yabuno, T. Yamashita, H. Terai, M. Koashi, T. Mukai, T. Yamamoto, and N. Imoto, *Nat. Commun.* **9**, 1997 (2018).
- [43] H. Levine, A. Keesling, A. Omran, H. Bernien, S. Schwartz, A. S. Zibrov, M. Endres, M. Greiner, V. Vuletić, and M. D. Lukin, *Phys. Rev. Lett.* **121**, 123603 (2018).
- [44] J. D. Wong-Campos, S. A. Moses, K. G. Johnson, and C. Monroe, *Phys. Rev. Lett.* **119**, 230501 (2017).
- [45] D. Hucul, I. V. Inlek, G. Vittorini, C. Crocker, S. Debnath, S. M. Clark, and C. Monroe, *Nat. Phys.* **11**, 37 (2015).

- [46] K. Stannigel, P. Rabl, A. S. Sørensen, P. Zoller, and M. D. Lukin, *Phys. Rev. Lett.* **105**, 220501 (2010)
- [47] C. Genes, D. Vitali, and P. Tombesi, *Phys. Rev. A* **77**, 050307(R) (2008).
- [48] J.-M. Raimond, M. Brune, and S. Haroche, *Rev. Mod. Phys.* **73**, 565 (2001).
- [49] L. Zhou, Y. Han, J. Jing, and W. Zhang, *Phys. Rev. A* **83**, 052117 (2011).
- [50] E. A. Sete and H. Eleuch, *J. Opt. Soc. Am. B* **32**, 971 (2015).
- [51] W. Ge, M. Al-Amri, H. Nha, and M. S. Zubairy, *Phys. Rev. A* **88**, 052301 (2013).
- [52] H. Xiong and Y. Wu, *Appl. Phys. Rev.* **5**, 031305 (2018).
- [53] W. Nie, A. Chen, and Y. Lan, *Phys. Rev. A* **93**, 023841 (2016).
- [54] W. Nie, A. Chen, and Y. Lan, *Opt. Express* **25**, 32931 (2017).
- [55] H. Xiong, L.-G. Si, X.-Y. Lü, X. Yang, and Y. Wu, *Opt. Lett.* **38**, 353 (2013).
- [56] Z.-X. Liu, H. Xiong, and Y. Wu, *Phys. Rev. A* **97**, 013801 (2018).
- [57] H. Xiong, L.-G. Si, X.-Y. Lü, and Y. Wu, *Opt. Express* **24**, 5773 (2016).
- [58] X. Li, W. Nie, A. Chen, and Y. Lan, *Phys. Rev. A* **96**, 063819 (2017).
- [59] W. Nie, A. Chen, Y. Lan, Q. Liao, and S. Zhu, *J. Phys. B: At., Mol. Opt. Phys.* **49**, 025501 (2015).
- [60] W. Nie, Y. Lan, Y. Li, and S. Zhu, *Phys. Rev. A* **86**, 063809 (2012).
- [61] W. Nie, Y. Lan, Y. Li, and S. Zhu, *Sci. China: Phys., Mech. Astron.* **57**, 2276 (2014).
- [62] A. Chen, W. Nie, L. Li, W. Zeng, Q. Liao, and X. Xiao, *Opt. Commun.* **403**, 97 (2017).
- [63] R. Benguria and M. Kac, *Phys. Rev. Lett.* **46**, 1 (1981).
- [64] G. A. T. Pender, P. F. Barker, Florian Marquardt, J. Millen, and T. S. Monteiro, *Phys. Rev. A* **85**, 021802(R) (2012).
- [65] V. Giovannetti and D. Vitali, *Phys. Rev. A* **63**, 023812 (2001).
- [66] A. Xuereb and M. Paternostro, *Phys. Rev. A* **87**, 023830 (2013).
- [67] O. Romero-Isart, M. L. Juan, R. Quidant, and J. I. Cirac, *New J. Phys.* **12**, 033015 (2010).
- [68] O. Romero-Isart, A. C. Pflanzer, M. L. Juan, R. Quidant, N. Kiesel, M. Aspelmeyer, and J. I. Cirac, *Phys. Rev. A* **83**, 013803 (2011).
- [69] M. O. Scully and M. S. Zubairy, *Quantum Optics* (Cambridge University Press, London, 1997).
- [70] E. X. DeJesus and C. Kaufman, *Phys. Rev. A* **35**, 5288 (1987).
- [71] G. Vidal and R. F. Werner, *Phys. Rev. A* **65**, 032314 (2002).